Universal Approximation Theorem and Deep Learning for the Solution of Frequency Domain Electromagnetic Scattering Problems

Ji-Yuan Wang and Xiao-Min Pan

Abstract—Unlike the universal approximation theorems for functions mapping from a real-valued (RV) vector to a RV number or from a complex-valued (CV) vector to a CV number, in the field of electromagnetism, we need to approximate functions mapping from a RV vector to a CV number when we consider the electric field as a function of the spatial coordinate in the frequency domain. Typically, CV numbers contain phase information. When such phase information is handled properly, the performance of the neural networks (NNs) can be improved. This work derives a universal approximation theorem for functions mapping from a RV vector to a CV number. A deep NN, named as HV-DL, is designed accordingly, which consists of a RV input layer, a RV module containing two branches, a CV module and a CV output layer. The proposed universal approximation theorem is verified by numerical experiments on the HV-DL solution of the two-dimensional (2-D) electric field integral equation (EFIE). To integrate the underlying physics of electromagnetic scattering into the proposed HV-DL, the loss function is computed according to the EFIE.

Index Terms—Physics-informed neural networks (PINNs), electromagnetic (EM) scattering, deep learning (DL), integral equations.

I. INTRODUCTION

IN recent years, deep learning (DL) [1]–[3] has emerged as a promising technique for solving partial differential equations (PDEs) by utilizing neural networks (NNs) to replace the whole or some nonlinear process of the traditional numerical solver. One attractive virtue of such methodology is that DL can integrate physical laws and data-driven approaches together. Such integration has been shown its accuracy, reliability, and interpretability of predictions in various applications [4]–[9]. When DL is taken as a numerical solver, including a computational electromagnetic (EM) one, NNs are typically regarded as function approximators [10]–[14], functional approximators [15]–[20] or operator approximators [21], [22]. In this work, we are interested in taking NNs as function approximators where the EM data is regarded as the function with respect to the spatial coordinate. The mathematical proof that NNs have the ability to approximate functions has been presented in the universal approximation theorem, whose development has a long history [23]–[33].

Initially, attention was focused on shallow architectures involving only a single hidden layer. Such a NN with the

sigmoidal activation function in the hidden layer has the capability to approximate continuous or other types of functions defined on a compact set in $\mathbb{R}^n$ [23]. It was subsequently proved that radial-basis-function (RBF) networks having a single hidden layer were capable of universal approximation [24]. The universal approximation theorems with some other special activation functions were discussed in [25]. A more general case, a shallow NN with the Tauber-Wiener (TW) activation function being capable of universal approximation, was proved in [26]. In fact, the commonly used activation functions like the rectified linear unit (ReLU), sigmoid, tanh, et. al. [27], are all TW functions.

Compared to shallow NNs, deep ones are more popularly utilized. In [28], it was proved that multilayer feedforward networks featured by an appropriately smooth hidden layer activation function, such as the sigmoid, were capable of achieving arbitrarily accurate approximation to an arbitrary function as well as its derivatives. The required hidden layer activation function of multilayer feedforward networks was extended to a non-sigmoid case in [29]. More details about the approximation theorem of the multilayer networks can be found in [30]. The aforementioned classic universal approximation theorem addressed the case of NNs with arbitrary width and bounded depth. In contrast, the scenario for networks of bounded width and arbitrary depth was investigated in [31].

As we know, the phase information is important in the EM data [15], [34]. If phase information was properly treated, the classification error can be further reduced for the polarimetric SAR imaging applications [35]. In [36], complex-valued (CV) NNs were proved to handle phase information more effectively than real-valued (RV) ones. In addition to the development of aforementioned universal approximation theorems where the input, weights, biases, output and activation functions of NNs are all RV, researches on the CV universal approximation theorem have been conducted. It was shown that a CV shallow feedforward NN, employing a subset of complex elementary transcendental functions as the activation function, can achieve universal approximation of any CV mapping to an arbitrary accuracy [32]. In [33], the universal approximation property was proved to be held as long as the activation function was neither a polynomial, a holomorphic function, nor an antiholomorphic function for CV deep as well as shallow NNs.

Except for functions corresponding to existing universal approximation theorems, which map from a RV vector to a RV number or from a CV vector to a CV number, we also require functions to map from a RV vector to a CV number.

A typical application is to obtain the CV electric field in the frequency domain with respect to the spatial coordinate. However, to the best of our knowledge, no report on this topic is publicly available. This work will fill this gap by investigating the universal approximation theorem in terms of the function mapping from a RV vector to a CV number. In addition, a deep NN called HV-DL is designed to validate the theorem. The proposed HV-DL contains a RV input layer, a RV module with two branches, a CV module and a CV output layer. The two branches in the RV module share their weights except the biases.

There are various approaches available for training the HV-DL. Among them, the physics-informed neural network (PINN) [37]–[39] is a popular one, which can gracefully incorporate the physical knowledge, always in the form of PDEs, into NNs. In fact, the PINN paradigm has already shown its potential in EM analysis [10]–[13], [40]–[42], although the employed NNs were almost RV ones. Based on these observations, similar to the report in [11], this work employs the methodology of PINNs to train the HV-DL. The main contributions of this work are as follows:

1) A universal approximation theorem for functions mapping from a RV vector to a CV number is proved.
2) According to the developed theorem, a so-called HV-DL is specifically designed to handle phase information explicitly.
3) A comparative study is conducted where the performance of the HV-DL is investigated against the traditional RV NNs and CV NNs.

The rest of the paper is as follows. In Section II, the EM scattering is reviewed. In Section III, the universal approximation theorem for functions that map from a RV vector to a CV number is developed and the HV-DL is proposed. In Section IV, numerical experiments are carried out to validate the developed universal approximation theorem. The performance of the HV-DL is also demonstrated here. Conclusions are given in Section V.

II. PROBLEM STATEMENT

A 2-D nonmagnetic transverse magnetic (TM) case is considered in this work, as shown in Fig. 1. The dielectric scatterers are positioned in a domain $\mathcal{D} \in \mathbb{R}^2$ with homogeneous background, i.e., the free space. Suppose the relative permittivity of the scatterer at $\mathbf{r}$ is $\varepsilon_r(\mathbf{r})$, the electric field integral equation (EFIE) describing the scattering under the illumination of a harmonic incident wave $\mathbb{E}_z^{\text{inc}}(\mathbf{r})$ with the time-factor being $e^{j\omega t}$ can be written as

$$
\mathbb{E}_z^{\text{tot}}(\mathbf{r}) = \mathbb{E}_z^{\text{inc}}(\mathbf{r}) \\
+ k_0^2 \int_{\mathcal{D}} G(\mathbf{r}, \mathbf{r}') (\varepsilon_r(\mathbf{r}') - 1) \mathbb{E}_z^{\text{tot}}(\mathbf{r}') d\mathbf{r}', \quad \mathbf{r} \in \mathcal{D}
$$

(1)

where $\mathbb{E}_z^{\text{tot}}(\mathbf{r})$ refers to the total electric field, k_0 is the wave number of the free space, $\mathbf{r}$ and $\mathbf{r}'$ denote the positions of the field and source point respectively, $G(\mathbf{r}, \mathbf{r}') = -\frac{j}{4} H_0^{(2)}(k_0 |\mathbf{r} - \mathbf{r}'|)$ is the 2-D Green's function in free space with $H_0^{(2)}(\cdot)$ representing the Hankel function of the second
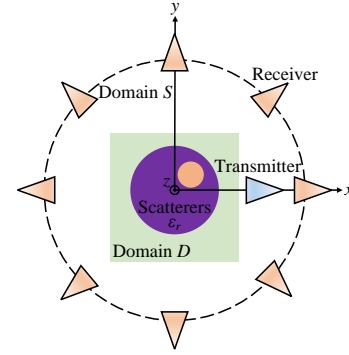

Fig. 1. Geometry of EM scattering problems in the 2-D case.

kinds of order zero and $j = \sqrt{-1}$ referring to the imaginary unit.

The scattered electric field can be measured by the receivers in the domain $\mathcal{S} \in \mathbb{R}^2$:

$$
\mathbb{E}_z^{\text{sca}}(\mathbf{r}) = k_0^2 \int_{\mathcal{S}} G(\mathbf{r}, \mathbf{r}') (\varepsilon_r(\mathbf{r}') - 1) \mathbb{E}_z^{\text{tot}}(\mathbf{r}') d\mathbf{r}', \quad \mathbf{r} \in \mathcal{S}
$$

(2)

where $\mathbb{E}_z^{\text{sca}}(\mathbf{r})$ denotes the scattered electric field.

The above EM scattering problem is widely solved by the method of moments (MoM) [43]–[45]. After discretizing the computational domain $\mathcal{D}$ and defining the contrast as $\chi(\mathbf{r}') = \varepsilon_r(\mathbf{r}') - 1$, the MoM matrix system arising from Eq. (1) can be written as,

$$
\mathbf{E}^{\text{tot}} = \mathbf{E}^{\text{inc}} + \mathbf{G}_{\mathcal{D}} \cdot \boldsymbol{\chi} \cdot \mathbf{E}^{\text{tot}},
$$

(3)

where $\mathbf{E}^{\text{tot}}$ and $\mathbf{E}^{\text{inc}}$ are vectors of the discrete total and incident electric field respectively, $\boldsymbol{\chi}$ is the diagonal matrix storing the contrast of each sub-domain, and $\mathbf{G}_{\mathcal{D}}$ is the matrix of the free space Green's function in the domain $\mathcal{D}$.

After $\mathbf{E}^{\text{tot}}$ is obtained by solving Eq. (3), the discrete scattered electric field of any observation region can be calculated:

$$
\mathbf{E}^{\text{sca}} = \mathbf{G}_{\mathcal{S}} \cdot \boldsymbol{\chi} \cdot \mathbf{E}^{\text{tot}},
$$

(4)

where $\mathbf{G}_{\mathcal{S}}$ is the matrix of the free space Green's function in the domain $\mathcal{S}$.

III. THE PROPOSED METHOD

This section discusses the universal approximation theorem for functions mapping from a RV vector to a CV number. The so-called HV-DL based on the established universal approximation theorem is presented accordingly.

A. Approximation to Functions

We start with introducing the TW function [26, Definition 2]. If a continuous or discontinuous function $g : \mathbb{R} \to \mathbb{R}$ satisfies that all the linear combinations $\sum_{i=1}^{N} a_i g(\lambda_i r + \theta_i)$, where $\lambda_i \in \mathbb{R}$, $\theta_i \in \mathbb{R}$, $a_i \in \mathbb{R}$ and $i = 1, 2, \cdots, N$, are dense in every $\mathbb{B}[a, b]$, then g is called a Tauber-Wiener (TW) function. Here, $\mathbb{B}[a, b]$ denotes Banach space of all continuous functions defined on $[a, b]$ with norm $\|f\|_{\mathbb{B}[a,b]} = \max_{x \in [a,b]} |f(x)|$. The classic universal approximation theorem presented in [26]

shows that a shallow NN with a TW function in the hidden layer is capable of universal approximation from a RV vector to a RV number.

Base on the classic theorem, the following statement can be obtained for functions mapping from a RV vector to a CV number. Suppose that $\mathbb{K}$ is a compact set in $\mathbb{R}^n$, $\mathbb{U}$ is a compact set in $\mathbb{B}(\mathbb{K})$ where $\mathbb{B}(\mathbb{K})$ denotes Banach space of all continuous functions defined on $\mathbb{K}$, with norm $\|f\|_{\mathbb{B}(\mathbb{K})} = \max_{x \in \mathbb{K}} |f(x)|$, and $\sigma \in$ (TW), then for any $\epsilon > 0$, there exist a positive integer $N \in \mathbb{N}^*$, RV numbers $\eta_i, \rho_i \in \mathbb{R}$, vectors $\mathbf{w}_i \in \mathbb{R}^n$ that are independent of the CV function $f \in \mathbb{B}(\mathbb{K})$ and CV constants $c_i(f) \in \mathbb{C}$ depending on f, where $i = 1, \cdots, N$, such that

$$\left| f(\mathbf{r}) - \sum_{i=1}^{N} c_i(f) \left(\sigma \left(\mathbf{w}_i^T \cdot \mathbf{r} + \eta_i \right) \right. \right. \tag{5}$$
$$\left. \left. + j\sigma \left(-\mathbf{w}_i^T \cdot \mathbf{r} + \rho_i \right) \right) \right| < \epsilon$$

holds for all $\mathbf{r} \in \mathbb{K}$ and $f \in \mathbb{U}$. The detailed proof can be found in Appendix A.

Equation (5) provides a shallow NN structure that can treat the phase information explicitly when approximating functions mapping from a RV vector to a CV number. In practice, the deep networks always outperform the shallow ones [46]. To design a deep network for approximating functions that map from a RV vector to a CV number, a deep alternative of Eq. (5) is given in the following. Suppose that $\mathbb{K}$ is a compact set in $\mathbb{R}^n$, $\mathbb{U}$ is a compact set in $\mathbb{B}(\mathbb{K})$, then for any $\epsilon > 0$, there exist continuous vector functions $h : \mathbb{R}^n \to \mathbb{R}^m$ and $u : \mathbb{C}^m \to \mathbb{C}$, such that

$$\left| f(\mathbf{r}) - u\left(h_{(\mathbf{W}, \boldsymbol{\eta})}(\mathbf{r}) + jh_{(-\mathbf{W}, \boldsymbol{\rho})}(\mathbf{r}) \right) \right| < \epsilon \tag{6}$$

holds for all $\mathbf{r} \in \mathbb{K}$ and $f \in \mathbb{U}$. Functions $h_{(\cdot)}(\mathbf{r})$ and $u(\cdot)$ are the RV and CV multilayer feedforward NN respectively. The subscript $\mathbf{W}$ of $h_{(\cdot)}(\mathbf{r})$ represents learnable weights in the network $h_{(\cdot)}(\mathbf{r})$ with $\boldsymbol{\eta}$ and $\boldsymbol{\rho}$ the associated learnable biases.

It should be noted that all weights and biases in the RV layers are RV numbers and they are CV numbers in the CV layers.

B. HV-DL

A deep network can be designed according to Eq. (6), whose structure is shown in Fig. 2. The network has a RV input layer, a RV module containing two RV branch networks, a CV module and a CV output layer. The network is named as HV-DL as it has both RV and CV layers.

It should be noted that the two RV networks in the RV module have the same depth and width. Additionally, they can share their learnable weights except for the corresponding biases. The minus symbol in the subscript of $g_{(\cdot)}$ in Eq. (6) emphasizes this fact.

Suppose that the number of hidden layers in the RV module is denoted by L_{RV} layers and that in the CV module is by L_{CV} layers, the HV-DL has $(2 + L_{\text{RV}} + L_{\text{CV}})$ layers including the input and output layers. If $L_{\text{CV}} = 0$ and $L_{\text{RV}} = 1$, the HV-DL becomes a shallow NN which can be strictly described by Eq. (5). This shallow network is denoted by HV-NN for convenience, whose structure is depicted in Fig. 3.
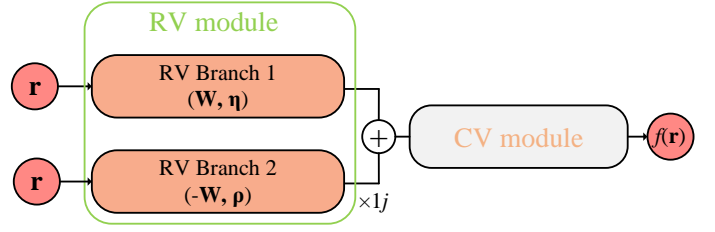

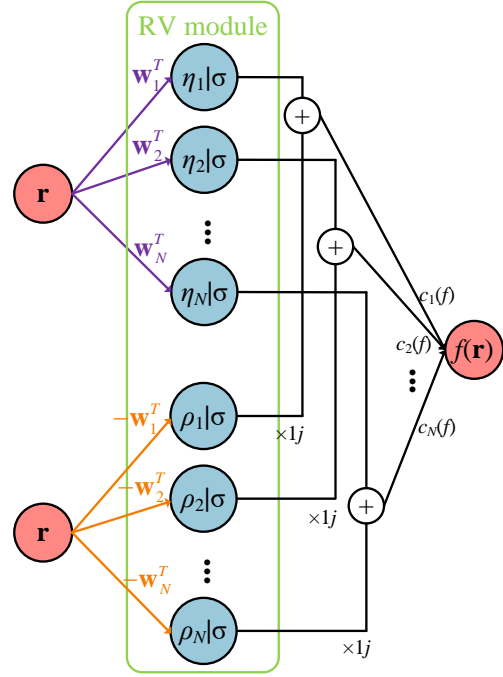Fig. 2. The configuration of the HV-DL.

Fig. 3. The configuration of the HV-NN.

According to Eq. (6), the mapping of the HV-DL is mathematically expressed as $\mathcal{N}(\mathbf{r}) : \mathbb{R}^2 \to \mathbb{C}$. Let $\mathcal{N}_{\text{real}}^{l_{\text{RV}}}$ and $\mathcal{N}_{\text{imag}}^{l_{\text{RV}}}$ stand for the l_{RV}-th layers of the two branches respectively ($l_{\text{RV}} = 1, 2, \cdots, L_{\text{RV}}$). Let us denote the learnable weight coefficients in the l_{RV}-th layer of two branches by $\mathbf{W}^{l_{\text{RV}}} \in \mathbb{R}^{N_{l_{\text{RV}}} \times N_{l_{\text{RV}}-1}}$ as well as the learnable biases by $\boldsymbol{\eta}^{l_{\text{RV}}} \in \mathbb{R}^{N_{l_{\text{RV}}}}$ and $\boldsymbol{\rho}^{l_{\text{RV}}} \in \mathbb{R}^{N_{l_{\text{RV}}}}$ respectively. As for the CV module, the learnable weights in the l_{CV}-th ($l_{\text{CV}} = 1, \cdots, L_{\text{CV}}$) layer are denoted by $\mathbf{C}^{l_{\text{CV}}} \in \mathbb{C}^{N_{l_{\text{CV}}} \times N_{l_{\text{CV}}-1}}$ and the corresponding learnable biases are denoted by $\mathbf{b}^{l_{\text{CV}}} \in \mathbb{C}^{N_{l_{\text{CV}}}}$. The weights and bias of the output layer are denoted by $\mathbf{C}^{\text{out}} \in \mathbb{C}^{1 \times N_{L_{\text{CV}}}}$ and $b^{\text{out}} \in \mathbb{C}$ respectively. For convenience, the layers in the HV-DL are increasingly indexed from the left/input to the right/output. For example, the 1-st layer is the RV input layer and the $(2 + L_{\text{RV}} + L_{\text{CV}})$-th layer is the CV output layer. Given a nonlinear RV activation function σ_{RV} and a nonlinear CV activation function σ_{CV}, the HV-DL is defined as follows.

- RV input layer: $\mathcal{N}^1(\mathbf{r}) = \mathbf{r} \in \mathbb{R}^2$.
- RV module:

$$\mathcal{N}_{\text{real}}^{l_{\text{RV}}+1}(\mathbf{r}) = \sigma_{\text{RV}} \left(\mathbf{W}^{l_{\text{RV}}} \cdot \mathcal{N}_{\text{real}}^{l_{\text{RV}}}(\mathbf{r}) + \boldsymbol{\eta}^{l_{\text{RV}}} \right) \in \mathbb{R}^{N_{l_{\text{RV}}}}$$
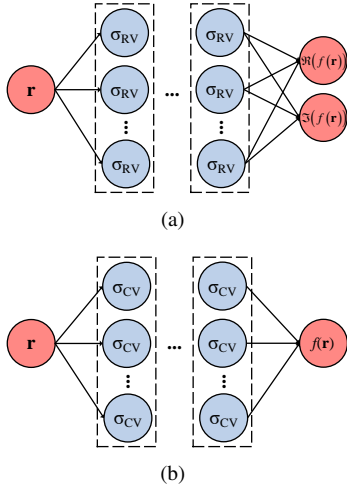
Fig. 4. The typical configurations of the multilayer feedforward NN. (a) RV-DL. (b) CV-DL.

and

$$\mathcal{N}_{\text{imag}}^{l_{\text{RV}}+1}(\mathbf{r}) = \sigma_{\text{RV}} \left(-\mathbf{W}^{l_{\text{RV}}} \cdot \mathcal{N}_{\text{imag}}^{l_{\text{RV}}}(\mathbf{r}) + \boldsymbol{\rho}^{l_{\text{RV}}} \right) \in \mathbb{R}^{N_{l_{\text{RV}}}},$$

for $1 \leq l_{\text{RV}} \leq L_{\text{RV}}$, where $\mathcal{N}_{\text{real}}^1(\mathbf{r}) = \mathcal{N}_{\text{imag}}^1(\mathbf{r}) = \mathcal{N}^1(\mathbf{r})$.

- Combination:

$$\mathcal{N}^{1+L_{\text{RV}}}(\mathbf{r}) = \mathcal{N}_{\text{real}}^{1+L_{\text{RV}}}(\mathbf{r}) + j\mathcal{N}_{\text{imag}}^{1+L_{\text{RV}}}(\mathbf{r}) \in \mathbb{C}^{N_{L_{\text{RV}}}}.$$

- CV module:

$$\mathcal{N}^{1+L_{\text{RV}}+l_{\text{CV}}}(\mathbf{r}) = $$
$$\sigma_{\text{CV}} \left(\mathbf{C}^{l_{\text{CV}}} \cdot \mathcal{N}^{L_{\text{RV}}+l_{\text{CV}}}(\mathbf{r}) + \mathbf{b}^{l_{\text{CV}}} \right) \in \mathbb{C}^{N_{l_{\text{CV}}}},$$

for $1 \leq l_{\text{CV}} \leq L_{\text{CV}}$.

- CV output layer:

$$\mathcal{N}^{2+L_{\text{RV}}+L_{\text{CV}}}(\mathbf{r}) = \mathbf{C}^{\text{out}} \cdot \mathcal{N}^{1+L_{\text{RV}}+L_{\text{CV}}}(\mathbf{r}) + b^{\text{out}} \in \mathbb{C}.$$

Although it does not appear in Eqs. (5) and (6), adding a bias in the output layer may improve the performance. That is the reason why a bias is included in the output layer of the HV-DL.

This work employs the ReLU activation function for the RV module and its CV form $\mathbb{C}$ReLU [36] for the CV module. The employed $\mathbb{C}$ReLU can be written as,

$$\mathbb{C}\text{ReLU}(z) = \text{ReLU}\left(\Re\left(z \right) \right) + j\text{ReLU}\left(\Im\left(z \right) \right), \quad (7)$$

where z is a CV number, $\Re\left(\cdot \right)$ and $\Im\left(\cdot \right)$ give the real and imaginary components of the corresponding CV number.

C. How to Train the HV-DL

There are several approaches available to train the specifically designed HV-DL. Among them, this work selects the PINN diagram as it can encode the underlying physics into the employed NN by the governing equations. Similar to the report in [11], this work integrates the integral equation in its EFIF's form, see Eq. (1), into the loss function, which is expressed as

$$\mathcal{L}(\boldsymbol{\theta}) = \frac{\left\| \mathbf{E}_{\text{Pred}}^{\text{tot}} - \mathbf{E}^{\text{inc}} - \mathbf{G}_D \cdot \boldsymbol{\chi} \cdot \mathbf{E}_{\text{Pred}}^{\text{tot}} \right\|_2^2}{M}, \quad (8)$$

where $\boldsymbol{\theta}$ is the set of parameters of the HV-DL, $\mathbf{E}_{\text{Pred}}^{\text{tot}} \in \mathbb{C}^{M \times 1}$ is the total electric field obtained from the HV-DL, M is the number of sampled sub-domains and $\|\cdot\|_2$ denotes the ℓ_2 norm of a vector.

D. Remarks

1) Network Structures: Two other common employed network structures are given in Figs. 4(a) and 4(b). They are denoted by RV-DL and CV-DL, respectively. The RV-DL treats the phase information implicitly by generating the real- and imaginary-components of the electric field. In comparison with the proposed HV-DL, no weight is shared as only one RV branch is employed. Contrastively, the CV-DL handles the phase information in a fully explicit manner by employing CV weights and biases in the NN.

In our implementations, the structure of the resultant HV-DL is not identical to that of the CV-DL even when $L_{\text{RV}} = 0$ due to the presence of the input layer, which is implicitly contained in the RV module. At the same time the structure of the resultant HV-DL is not identical to that of the RV-DL even when $L_{\text{CV}} = 0$ for the similar reason.

2) The Number of Learnable Parameters: Due to the additional knowledge on the learnable parameters of the two branches in the RV module, the number of learnable parameters, denoted by n_{para}, in the proposed HV-DL can be greatly reduced compared with the RV-DL and CV-DL.

Following the symbolic representation of the subsection III-B, the HV-DL has L_{RV} layers in the RV module and L_{CV} layers in the CV module. Suppose $n_{\text{HV}}^l (1 \leq l \leq 2 + L_{\text{RV}} + L_{\text{CV}})$ denotes the number of neurons in the l-th layer, we have

$$\begin{array}{l} n_{\text{HV}}^1 = 2 \\ n_{\text{HV}}^{2+L_{\text{RV}}+L_{\text{CV}}} = 1 \end{array}, \quad (9)$$

for the 2-D case in this work. For convenience, we assume that

$$\begin{array}{l} n_{\text{HV}}^2 = n_{\text{HV}}^3 = \cdots = n_{\text{HV}}^{1+L_{\text{RV}}} = n_{\text{neu, 1}} \\ n_{\text{HV}}^{L_{\text{RV}}+2} = n_{\text{HV}}^{L_{\text{RV}}+3} = \cdots = n_{\text{HV}}^{1+L_{\text{RV}}+L_{\text{CV}}} = n_{\text{neu,2}} \end{array}, \quad (10)$$

where $n_{\text{neu, 1}} \in \mathbb{N}^*$ and $n_{\text{neu, 2}} \in \mathbb{N}^*$ are both positive integers. In Eq. (10), n_{HV}^l counts the neurons of two branches. The total number of learnable parameters of the HV-DL is,

$$\begin{aligned} n_{\text{para}} = &(L_{\text{RV}}/4 - 1/4)n_{\text{neu,1}}^2 + (2L_{\text{CV}} - 2)n_{\text{neu,2}}^2 + \\ &(L_{\text{RV}} + 1)n_{\text{neu,1}} + (2L_{\text{CV}} + 2)n_{\text{neu,2}} + \\ &n_{\text{neu,1}}n_{\text{neu,2}} + 2 \end{aligned} \quad (11)$$

Here, the fact that the two branches share a same set of weights is taken into account during the process of counting the number of the learnable weights.

Similarly, we suppose that n_{RV}^l denotes the number of neurons in the l-th layer of a $(2 + L_{\text{RV}} + L_{\text{CV}})$-layered RV-DL and n_{CV}^l corresponds to that of the CV-DL counterpart. In a 2-D case, we have

$$\begin{array}{l} n_{\text{RV}}^1 = n_{\text{CV}}^1 = 2 \\ n_{\text{RV}}^{2+L_{\text{RV}}+L_{\text{CV}}} = 2n_{\text{CV}}^{2+L_{\text{RV}}+L_{\text{CV}}} = 2 \end{array}. \quad (12)$$
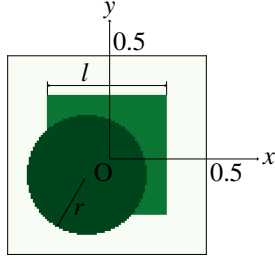
Fig. 5. The sketch of the investigated 2-D dielectric scatterer where the detailed information is shown in Table I.

TABLE I
CONFIGURATIONS OF THE SCATTERER IN FIG. 5.

	Center (m)	Size (m)	ε_r
Rectangular	(0, 0)	$l = 0.6$	3.5
Cylinder	(-0.1, -0.1)	$r = 0.3$	4.0

For convenience, we also let

$$n_{\text{RV}}^2 = n_{\text{RV}}^3 = \cdots = n_{\text{RV}}^{1+L_{\text{RV}}+L_{\text{CV}}} = n_{\text{neu},3}$$
$$n_{\text{CV}}^2 = n_{\text{CV}}^3 = \cdots = n_{\text{CV}}^{1+L_{\text{RV}}+L_{\text{CV}}} = n_{\text{neu},4}, \quad (13)$$

where $n_{\text{neu},3} \in \mathbb{N}^*$ and $n_{\text{neu},4} \in \mathbb{N}^*$ are both positive integers. Then, the total number of learnable parameters of the RV-DL is

$$n_{\text{para}} = (L_{\text{RV}}+L_{\text{CV}}-1)n_{\text{neu},3}^2+(L_{\text{RV}}+L_{\text{CV}}+4)n_{\text{neu},3}+2. \quad (14)$$

That of the CV-DL is

$$n_{\text{para}} = (2L_{\text{RV}}+2L_{\text{CV}}-2)n_{\text{neu},4}^2+(2L_{\text{RV}}+2L_{\text{CV}}+6)n_{\text{neu},4}+2. \quad (15)$$

If $n_{\text{neu},1} = 2n_{\text{neu},2} = n_{\text{neu},3} = 2n_{\text{neu},4} = n_{\text{neu}}$ with $n_{\text{neu}} \in \mathbb{N}^*$ a positive integer, the HV-DL has $(3L_{\text{RV}}/4 + L_{\text{CV}}/2 - 3/4)n_{\text{neu}}^2+2n_{\text{neu}}$ and $(L_{\text{RV}}/4-1/4)n_{\text{neu}}^2+n_{\text{neu}}$ fewer learnable parameters than its RV-DL and CV-DL counterparts. It should be noted that the HV-DL does not necessarily save training time although it can save memory. The reason lies in the fact that most of NNs are well-tuned for RV numbers instead of CV ones.

IV. NUMERICAL RESULTS

The universal approximation theorem for functions mapping from a RV vector to a CV number is verified by numerical experiments on the HV-DL. During the verification process, the performance of the HV-DL is revealed. The NNs in this work are built by Pytorch [47]. In the training stage, the adaptive moment estimation method (Adam) [48] is employed to minimize the loss function shown in Eq. (8). The learning rate is initialized to 0.001. The change of the learning rate follows an exponential decay strategy with a decay coefficient of 0.9999, i.e., the learning rate for the i-th iteration is $l = l_{\text{ini}} \times \gamma^i$, where l_{ini} is the initial learning rate and γ is the decay coefficient. The total number of iterations is 60,000. The initialization of network weights follows the *Kaiming* uniform initialization [49] while the network biases are initialized to 0.

A uniform sampling is used to generate the training data. To say, the computational domain $\mathcal{D}$ is discretized by the rectangular cell of size 0.02 m and the sampled points are located at the center of the rectangular cells. To quantify the difference between the NN predictions and true values generated by the MoM in the testing stage, a relative error is defined as follows:

$$re = \frac{\|\mathbf{E}_{\text{Pred}}^{\text{tot}} - \mathbf{E}_{\text{MoM}}^{\text{tot}}\|_2}{\|\mathbf{E}_{\text{Pred}}^{\text{tot}}\|_2}, \quad (16)$$

where $\mathbf{E}_{\text{MoM}}^{\text{tot}} \in \mathbb{C}^{M \times 1}$ is the total electric field obtained from the MoM.

For studies in the subsections IV-A∼IV-C, a lossless scatterer as shown as Fig. 5 is employed, whose detailed information is given in Table I. The background is the rectangular free space centering at (0, 0) with the area of 1×1 m². The computations are limited to the scenario with a single incident angle of $0°$ under the working frequency of 300 MHz. The scattered electric field is sampled at 360 points that are uniformly located on a circle with a radius of 5 m.

The subsection IV-A carries out the study on the HV-NN where no CV module is equipped, which reveals the importance of the presence of the CV module by a comparison with the investigations in the subsequent three subsections. In the subsection IV-B, the performance of the HV-DL with the CV module equipped is studied by varying the depth of the HV-DL where its width is fixed. As the width of the network is also an important hyperparameter, the subsection IV-C investigates the performance of the HV-DL as a function of the width when the depth is fixed. To more comprehensively reveal the performance of the proposed HV-DL, computations on a set of scatterers with complex shapes are given in the subsection IV-D.

A. HV-DL With $L_{RV} = 1$ and $L_{CV} = 0$

The performance of the HV-DL with $L_{\text{RV}} = 1$ and $L_{\text{CV}} = 0$ is studied by varying the width of the hidden layer. To reach a comparative study, computations by the shallow RV-DL and CV-DL with only one hidden layer are conducted. The width, namely, the number of neurons, varies from 100 to 4000 in terms of the RV-DL. Table II records n_{para}'s as well as re's for all computations. It seems that the HV-DL performs inferior to the RV-DL and CV-DL.

The absence of a CV module in the HV-NN contributes to degraded performance, as will be revealed in the following subsections.

B. HV-DL With Different Depths

No CV module can exist in the HV-NN due to the limited depth. As a result, the potential of the HV-DL cannot be fully revealed by the HV-NN. This subsection aims to more comprehensively reveal the performance of the HV-DL by increasing its depth. In particular, by varying the depth from 4 to 11, the HV-DL is investigated against the RV-DL and CV-DL. In all computations, we set $n_{\text{neu},1} = 2n_{\text{neu},2} = n_{\text{neu},3} = 2n_{\text{neu},4} = 100$. By such a choice, the differences in terms of n_{para}'s among the three NNs are minimized to the largest

TABLE II
COMPUTATIONS OF THE HV-NN. NOTATIONS ARE DEFINED IN SECTION III-D.

RV-DL (One Hidden Layer)			CV-DL (One Hidden Layer)			HV-NN		
$n_{\text{neu,3}}$	n_{para}	re (‰)	$n_{\text{neu,4}}$	n_{para}	re (‰)	$n_{\text{neu, 1}}$	n_{para}	re (‰)
100	502	73.6	50	402	102.9	100	302	125.7
200	1,002	55.7	100	802	73.8	200	602	109.8
500	2,502	17.1	250	2,002	37.8	500	1,502	49.4
1,000	5,002	17.2	500	4,002	35.7	1,000	3,002	50.0
2,000	10,002	15.3	1,000	8,002	28.7	2,000	6,002	54.0
3,000	15,002	12.2	1,500	12,002	31.7	3,000	9,002	67.4
4,000	20,002	20.8	2,000	16,002	33.4	4,000	12,002	78.4

TABLE III
COMPUTATIONS OF THE HV-DL. NOTATIONS ARE DEFINED IN
SECTION III-D.

$L_{\text{RV}} + L_{\text{CV}}$	HV-DL			
	L_{RV}	L_{CV}	n_{para}	re (‰)
2	1	1	5,402	20.5
3	1	2	10,502	11.1
4	1	3	15,602	9.0
5	2	3	18,202	7.5
6	5	1	15,802	5.6
7	6	1	18,402	4.8
8	5	3	26,002	4.5
9	6	3	28,602	3.7

TABLE IV
COMPUTATIONS OF THE RV-DL. IN THE TABLE, n_{DL} IS THE NUMBER OF
HIDDEN LAYERS. OTHER NOTATIONS ARE DEFINED IN SECTION III-D.

n_{DL}	RV-DL	
	n_{para}	re (‰)
4	10,602	11.6
5	20,702	8.1
6	30,802	5.4

TABLE V
COMPUTATIONS OF THE CV-DL. IN THE TABLE, n_{DL} IS THE NUMBER OF
HIDDEN LAYERS. OTHER NOTATIONS ARE DEFINED IN SECTION III-D.

n_{DL}	CV-DL	
	n_{para}	re (‰)
4	5,502	20.6
5	10,602	10.7
6	15,702	11.2
7	20,802	8.5
8	25,902	8.1
9	31,002	8.5

extent. In fact, even when $L_{\text{RV}} + L_{\text{CV}}$ is fixed, a couple of combinations of different RV and CV module implementations can be obtained. These combinations will make the resultant HV-DLs having different n_{para}'s. Such differences can be obviously seen in Table III where re's as well as n_{para}'s for the HV-DL computations are detailed. For the RV-DL and CV-DL computations, the detailed information can be found in Table IV and V.

As highlighted in Tables III, IV and V, the HV-DL can outperform the RV-DL and CV-DL when it has a comparable n_{para} with the latter two NNs. It is worth noting that Table III only show the results of the HV-DL with the relative smaller re values. A complete list can be found in Table B1 in Appendix B. From Table B1, it can be found that $L_{\text{CV}} = 3$ can always make the HV-DL perform well. Based on this observation, in what follows, we will fix L_{CV} at 3.

TABLE VI
COMPUTATIONS OF THE HV-DL WITH $L_{\text{RV}} = 6$ AND $L_{\text{CV}} = 3$ BY
VARYING THE WIDTH OF THE RV MODULE WHILE THAT OF THE CV
MODULE IS FIXED AT 50. NOTATIONS ARE DEFINED IN SECTION III-D.

	$n_{\text{neu,1}}$	n_{para}	re (‰)
	80	22,962	4.9
	100	28,602	3.7
	120	35,242	3.5
HV-DL	140	42,882	3.3
	160	51,522	2.7
	180	61,162	2.3
	200	71,802	2.5

TABLE VII
COMPUTATIONS OF THE HV-DL WITH $L_{\text{RV}} = 6$ AND $L_{\text{CV}} = 3$ BY
VARYING THE WIDTH OF THE CV MODULE WHILE THAT OF THE RV
MODULE IS FIXED AT 100. NOTATIONS ARE DEFINED IN SECTION III-D.

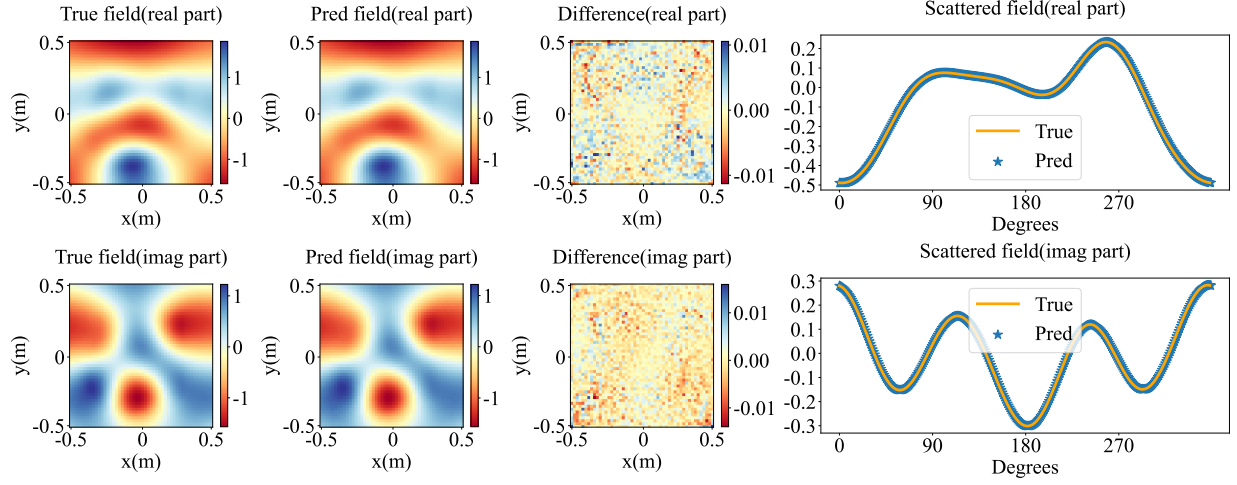|	$n_{\text{neu,2}}$	n_{para}	re (‰)
	40	23,922	4.6
	50	28,602	3.7
	60	34,082	3.7
HV-DL	70	40,362	3.4
	80	47,442	3.5
	90	55,322	2.1
	100	64,002	2.3

Fig. 6. The predicted results of the HV-DL with $L_{RV} = 6$ and $L_{CV} = 3$ on the investigated scatterer shown in Fig. 5. The 1st column is the real and imaginary parts of the true total field computed by the MoM. The 2nd column gives the real and imaginary parts of the predicted total field. The 3rd column shows the differences between true and predicted results. The last column are the true and predicted scattered field in $\phi \in [0°, 360°]$.

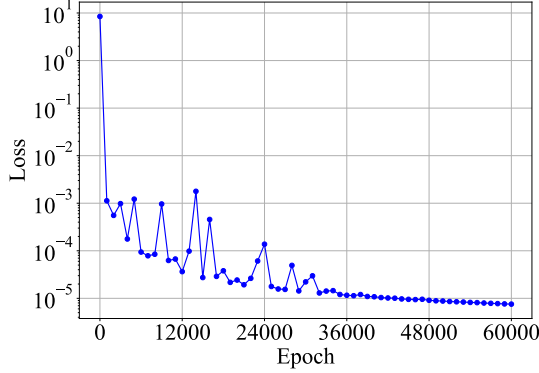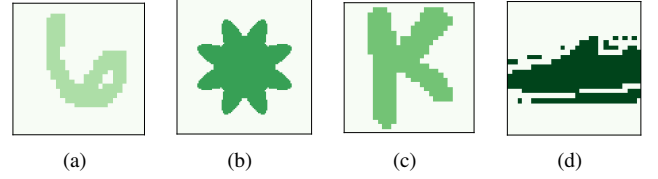Fig. 7. Losses of the HV-DL with $L_{RV} = 6$ and $L_{CV} = 3$ for the scatterer shown in Fig. 5.

Fig. 8. The sketch of the investigated 2-D dielectric objects whose detailed information is presented in Table VIII. (a) Scatterer 1. (b) Scatterer 2. (c) Scatterer 3. (d) Scatterer 4.

The performance of the HV-DL with $L_{RV} = 6$ and $L_{CV} = 3$ is additionally checked by the predicted total and scattered electric fields as shown in Fig. 6. It can be seen that both the predicted total and scattered electric fields agree well with their counterparts obtained by the MoM. The trajectory of losses recorded per 1,000 iterations are provided in Fig. 7. It is shown that the final loss can be smaller than $10e^{-5}$.
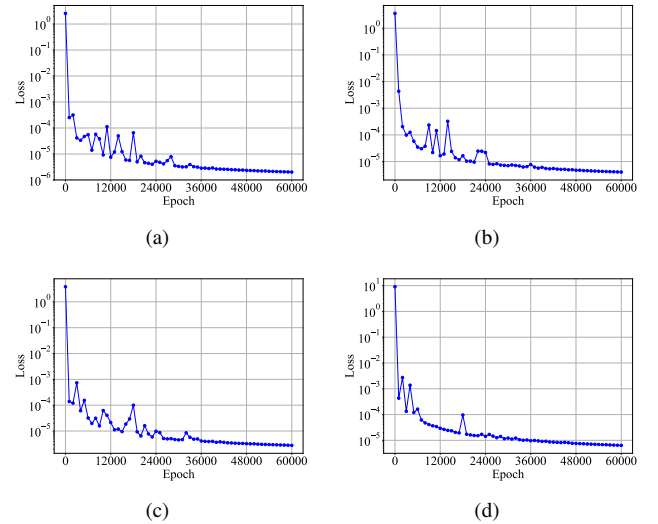

Fig. 9. Trajectories of losses for the HV-DL associated with the four investigated scatterers shown in Fig. 8. (a) Scatterer 1. (b) Scatterer 2. (c) Scatterer 3. (d) Scatterer 4.

TABLE VIII
THE COMPUTATIONAL CONFIGURATIONS AND re'S ASSOCIATED WITH THE SCATTERERS IN FIG. 8.

	Shape	ε_r	re (‰)
Scatterer 1	"6"	2.0	2.1
Scatterer 2	Flower	3.0	2.8
Scatterer 3	"K"	2.5+j0.5	3.2
Scatterer 4	Shoes	5.0+j1.0	4.4

C. HV-DL With Different Widths

By fixing $L_{RV} = 6$ and $L_{CV} = 3$, the performance of the HV-DL is investigated by varying the width of the hidden layers. Two set of computations are carried out. In one set, the number of neurons in each single hidden layer of the RV
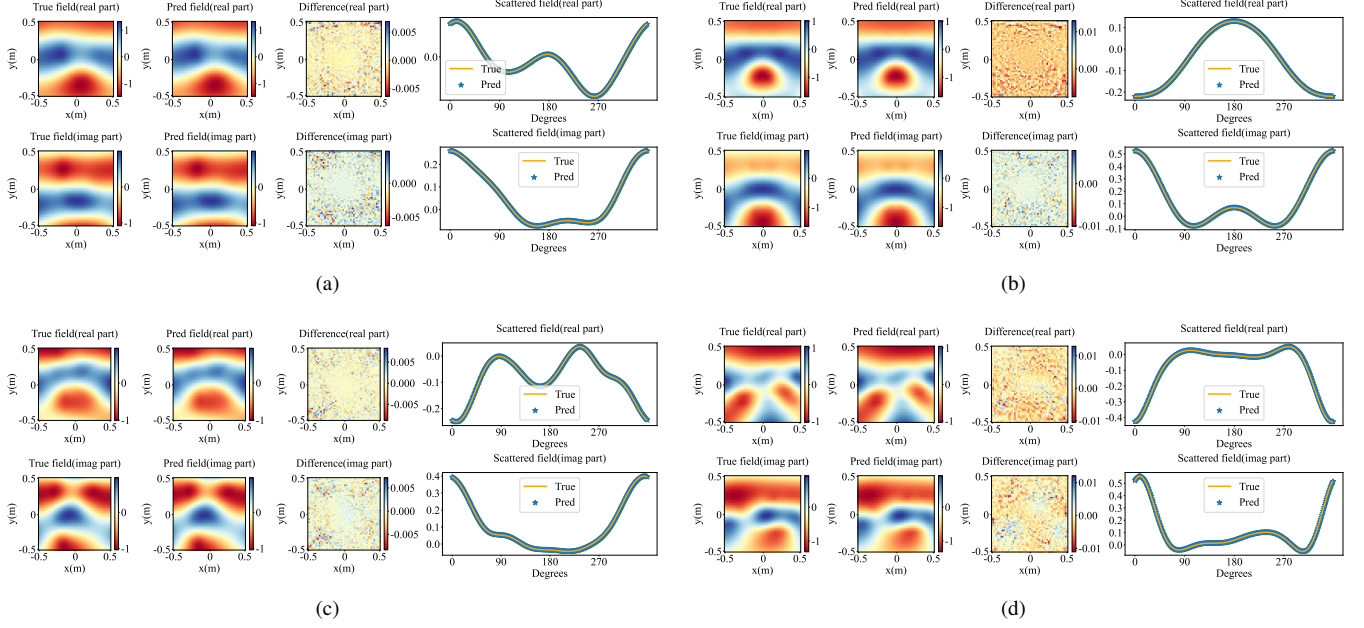
Fig. 10. The predicted results of the HV-DL with $L_{RV} = 6$ and $L_{CV} = 3$ on different scatterers shown in Fig. 8. The 1st column is the real and imaginary parts of the true total field computed by the MoM. The 2nd column gives the real and imaginary parts of the predicted total field. The 3rd column shows the differences between true and predicted results. The last column are the true and predicted scattered field in $\phi \in [0°, 360°]$. (a) Scatterer 1. (b) Scatterer 2. (c) Scatterer 3. (d) Scatterer 4.

module is increased from 80 to 200 while their CV counterpart remains fixed at 50. In the other set, the number of neurons in each single hidden layer of the CV module is increased from 40 to 100 while their RV counterpart remains fixed at 100.

Tables VI and VII present the associated results in 60,000 iterations respectively. It can be seen that the re slightly reduces as the width increase of either the RV or CV module. Based on the numerical experiments here and subsection IV-B, the performance of the HV-DL is not sensitive to the hyperparameters which are chosen here. In another word, the HV-DL can deliver nice prediction accuracy within a wide range of hyperparameters, which can alleviate the difficulty with respect to the hyperparameter selection.

D. Different Scatterers

To demonstrate the capability of the HV-DL, four scatterers with different geometry shapes are employed, as shown in Fig.8 and Table VIII.

An HV-DL with $L_{RV} = 6$ and $L_{CV} = 3$ is employed. In the computations, $n_{neu,1} = 2n_{neu,2} = 100$. The trajectories of losses associated with the four investigated scatterers are shown in Fig. 9. As can be seen, all the losses can reach $10e^{-5}$ within 60,000 iterations. The obtained total and scattered electric field results are presented in Fig. 10. It can be seen that both the predicted total and scattered electric field agree well with their counterparts obtained by the MoM.

V. CONCLUSION

The universal approximation theorem is investigated for functions mapping from a RV vector to a CV number. A specially designed NN, named as HV-DL, is obtained accordingly, where the some of the learnable weights can be shared to

save computational resource. The PINN-like training paradigm is utilized to train the developed HV-DL. Numerical results validate the analysis on the universal approximation theorem for functions mapping from a RV vector to a CV number.

APPENDIX A

According to [26, Lemma 4], that suppose $\mathbb{U}$ is a compact set in $\mathbb{B}_p[-1, 1]^n$ where $\mathbb{B}_p[-1, 1]^n$ stands for all periodic functions with period two with respect to their every variable, $B_R(f^*; \mathbf{r}) = \sum_{|\mathbf{m}| \leqslant R} \left(1 - \frac{|\mathbf{m}|^2}{R^2}\right)^\alpha c_\mathbf{m}(f^*) e^{j\pi \mathbf{m}^T \cdot \mathbf{r}}$ is the Bochner-Riesz means of Fourier series of f^* where $\mathbf{m} = [m_1, m_2, \cdots, m_n]^T$, $|\mathbf{m}|^2 = \sum_{i=1}^{n} |m_i|^2$ and $c_\mathbf{m}(f^*)$ are the Fourier coefficients of f^*, then for any $\epsilon > 0$, there is $R > 0$ such that

$$|B_R(f^*; \mathbf{r}) - f^*(\mathbf{r})| < \frac{\epsilon}{2} \tag{17}$$

holds for every $f^* \in \mathbb{U}$ and $\mathbf{r} \in [-1, 1]^n$, provided that $\alpha > (n-1)/2$.

According to Euler's formula, Eq. (17) can be rewritten as

$$\left| \sum_{|\mathbf{m}| \leqslant R} d_\mathbf{m} \left(\cos \pi \mathbf{m}^T \cdot \mathbf{r} + j \sin \pi \mathbf{m}^T \cdot \mathbf{r}\right) - f^*(\mathbf{r}) \right| < \frac{\epsilon}{2}, \tag{18}$$

where $d_\mathbf{m} = \left(1 - \frac{|\mathbf{m}|^2}{R^2}\right)^\alpha c_\mathbf{m}(f^*)$. Since there is a $\pi/2$ phase difference between the cosine function and the sine function,

Eq. (18) can also be written as

$$\left| \sum_{|\mathbf{m}| \leqslant R} d_{\mathbf{m}} \left(\cos \pi \mathbf{m}^T \cdot \mathbf{r} + j \cos \left(-\pi \mathbf{m}^T \cdot \mathbf{r} + \frac{\pi}{2} \right) \right) \right. \tag{19}$$
$$\left. - f^*(\mathbf{r}) \right| < \frac{\epsilon}{2}.$$

Since $\cos \pi \mathbf{m}^T \cdot \mathbf{r}$ is a continuous function in $[-1, 1]^n$, we can find a positive integer $M \in \mathbb{N}^*$, RV numbers $s_q, \xi_q, \eta_q \in \mathbb{R}$, $q = 1, 2, ..., M$, such that

$$\left| \sum_{q=1}^{M} s_q \sigma \left(\xi_q \pi \mathbf{m}^T \cdot \mathbf{r} + \eta_q \right) - \cos \pi \mathbf{m}^T \cdot \mathbf{r} \right| < \frac{\epsilon}{2\sqrt{2}L}, \tag{20}$$

where $L = \sum_{|\mathbf{m}| \leqslant R} |d_{\mathbf{m}}|$ and $\sigma \in$ (TW). Similarly, there are other RV numbers $\rho_q \in \mathbb{R}$, $q = 1, 2, ..., M$, such that

$$\left| \sum_{q=1}^{M} s_q \sigma \left(-\xi_q \pi \mathbf{m}^T \cdot \mathbf{r} + \rho_q \right) - \cos \left(-\pi \mathbf{m}^T \cdot \mathbf{r} + \frac{\pi}{2} \right) \right| \tag{21}$$
$$< \frac{\epsilon}{2\sqrt{2}L},$$

where $\rho_q = \frac{\pi}{2} \xi_q + \eta_q$.

Substituting Eqs. (20) and (21) into Eq. (18), we conclude that

$$\left| f^*(\mathbf{r}) - \sum_{|\mathbf{m}| \leqslant R} d_{\mathbf{m}} \left(\sum_{q=1}^{M} s_q \sigma \left(\xi_q \pi \mathbf{m}^T \cdot \mathbf{r} + \eta_q \right) \right. \right. \tag{22}$$
$$\left. \left. + j \sum_{q=1}^{M} s_q \sigma \left(-\xi_q \pi \mathbf{m}^T \cdot \mathbf{r} + \rho_q \right) \right) \right| < \epsilon.$$

The formula (22) is equivalent to that there are CV numbers $c_i(f^*) \in \mathbb{C}$ depending on f^*, a positive integer $N \in \mathbb{N}^*$ and vectors $\mathbf{w}_i \in \mathbb{R}^n$, $i = 1, 2, ..., N$, such that

$$\left| f^*(\mathbf{r}) - \sum_{i=1}^{N} c_i(f^*) \left(g \left(\mathbf{w}_i^T \cdot \mathbf{r} + \eta_i \right) \right. \right. \tag{23}$$
$$\left. \left. + j g \left(-\mathbf{w}_i^T \cdot \mathbf{r} + \rho_i \right) \right) \right| < \epsilon$$

holds for any $\mathbf{r} \in [-1, 1]^n$. According to [26, Lemma 3], suppose that $\mathbb{K}'$ is a compact set in $\mathbb{R}^n$, $\mathbb{V}$ is a compact set in $\mathbb{B}(\mathbb{K}')$, there are CV numbers $c_i(f) \in \mathbb{C}$ depending on f, a positive integer $N \in \mathbb{N}^*$ and vectors $\mathbf{w}_i \in \mathbb{R}^n$, such that

$$\left| f(\mathbf{r}) - \sum_{i=1}^{N} c_i(f) \left(g \left(\mathbf{w}_i^T \cdot \mathbf{r} + \eta_i \right) \right. \right. \tag{24}$$
$$\left. \left. + j g \left(-\mathbf{w}_i^T \cdot \mathbf{r} + \rho_i \right) \right) \right| < \epsilon$$

holds for any $\mathbf{r} \in \mathbb{K}'$ and $f \in \mathbb{V}$.

APPENDIX B

The computational information with respect to the HV-DL on predicting the scatterer's total electric field presented in Fig. 5 by varying the depth is detailed in Table B1. In the computations, $n_{\text{neu},1} = 2n_{\text{neu},2} = 100$. From the table, it can be seen that the proposed HV-DL can perform quite well when $L_{\text{RV}} + L_{\text{CV}}$ is larger than 3. For most cases, the best

TABLE B1
COMPUTATIONS OF THE HV-DL IN THE CASE OF DIFFERENT DEPTHS WHILE THE NEURONS OF EACH LAYER IN THE RV AND CV MODULE ARE FIXED TO 100 AND 50 RESPECTIVELY. IN THE TABLE, L_{RV} AND L_{CV} DENOTE THE NUMBER OF NETWORK LAYERS IN THE RV AND CV MODULE RESPECTIVELY. n_{PARA} IS THE NUMBER OF LEARNABLE PARAMETERS. re IS DEFINED AS EQ. (16).

$L_{\text{RV}} + L_{\text{CV}}$	L_{RV}	L_{CV}	n_{para}	re (‰)
2	1	1	5,402	20.5
	2	0	2,902	21.3
3	1	2	10,502	11.1
	2	1	8,002	11.7
	3	0	5,502	14.1
4	1	3	15,602	9.0
	2	2	13,102	12.7
	3	1	10,602	9.7
	4	0	8,102	12.2
5	1	4	20,702	8.4
	2	3	18,202	7.5
	3	2	15,702	7.7
	4	1	13,202	7.8
	5	0	10,702	8.5
6	1	5	25,802	11.3
	2	4	23,302	9.5
	3	3	20,802	6.1
	4	2	18,302	6.0
	5	1	15,802	5.6
	6	0	13,302	6.3
7	1	6	30,902	9.6
	2	5	28,402	7.3
	3	4	25,902	5.8
	4	3	23,402	5.4
	5	2	20,902	5.7
	6	1	18,402	4.8
	7	0	15,902	5.8
8	1	7	36,002	8.6
	2	6	33,502	6.3
	3	5	31,002	5.9
	4	4	28,502	5.8
	5	3	26,002	4.5
	6	2	23,502	4.6
	7	1	21,002	5.1
	8	0	18,502	5.5
9	1	8	41,102	9.2
	2	7	38,602	7.1
	3	6	36,102	6.8
	4	5	33,602	4.6
	5	4	31,102	5.3
	6	3	28,602	3.7
	7	2	26,102	4.1
	8	1	23,602	4.4
	9	0	21,102	4.2

performance of the HV-DL can always be reached by selecting $L_{CV} = 3$ when $L_{RV} + L_{CV}$ is larger than 4.

REFERENCES

[1] Y. LeCun, Y. Bengio, and G. Hinton, "Deep learning," *nature*, vol. 521, no. 7553, pp. 436–444, 2015.

[2] I. Goodfellow, Y. Bengio, and A. Courville, *Deep learning*. MIT press, 2016.

[3] D. E. Rumelhart, G. E. Hinton, and R. J. Williams, "Learning representations by back-propagating errors," *nature*, vol. 323, no. 6088, pp. 533–536, 1986.

[4] S. Cai, Z. Mao, Z. Wang, M. Yin, and G. E. Karniadakis, "Physics-informed neural networks (pinns) for fluid mechanics: A review," *Acta Mechanica Sinica*, vol. 37, no. 12, pp. 1727–1738, 2021.

[5] S. A. Faroughi, N. Pawar, C. Fernandes, M. Raissi, S. Das, N. K. Kalantari, and S. K. Mahjour, "Physics-guided, physics-informed, and physics-encoded neural networks in scientific computing," *arXiv preprint arXiv:2211.07377*, 2022.

[6] S. Cai, Z. Wang, S. Wang, P. Perdikaris, and G. E. Karniadakis, "Physics-informed neural networks for heat transfer problems," *Journal of Heat Transfer*, vol. 143, no. 6, p. 060801, 2021.

[7] G. S. Misyris, A. Venzke, and S. Chatzivasileiadis, "Physics-informed neural networks for power systems," in *2020 IEEE Power & Energy Society General Meeting (PESGM)*. IEEE, 2020, pp. 1–5.

[8] Y. Chen, L. Lu, G. E. Karniadakis, and L. Dal Negro, "Physics-informed neural networks for inverse problems in nano-optics and metamaterials," *Optics express*, vol. 28, no. 8, pp. 11 618–11 633, 2020.

[9] C. Song, T. Alkhalifah, and U. B. Waheed, "Solving the frequency-domain acoustic vti wave equation using physics-informed neural networks," *Geophysical Journal International*, vol. 225, no. 2, pp. 846–859, 2021.

[10] P. Zhang, Y. Hu, Y. Jin, S. Deng, X. Wu, and J. Chen, "A maxwell's equations based deep learning method for time domain electromagnetic simulations," *IEEE Journal on Multiscale and Multiphysics Computational Techniques*, vol. 6, pp. 35–40, 2021.

[11] J.-B. Zhang, D.-M. Yu, and X.-M. Pan, "Physics-informed neural networks for the solution of electromagnetic scattering by integral equations," in *2022 International Applied Computational Electromagnetics Society Symposium (ACES-China)*. IEEE, 2022, pp. 1–2.

[12] A. Khan and D. A. Lowther, "Physics informed neural networks for electromagnetic analysis," *IEEE Transactions on Magnetics*, vol. 58, no. 9, pp. 1–4, 2022.

[13] S. Qi and C. D. Sarris, "Hybrid physics-informed neural network for the wave equation with unconditionally stable time-stepping," *IEEE Antennas and Wireless Propagation Letters*, 2024.

[14] J.-J. Sun, S. Sun, Y. P. Chen, L. Jiang, and J. Hu, "Machine-learning-based hybrid method for the multilevel fast multipole algorithm," *IEEE Antennas and Wireless Propagation Letters*, vol. 19, no. 12, pp. 2177–2181, 2020.

[15] B.-W. Xue, R. Guo, M.-K. Li, S. Sun, and X.-M. Pan, "Deep learning equipped iterative solution of electromagnetic scattering from dielectric objects," *IEEE Transactions on Antennas and Propagation*, 2023.

[16] R. Guo, T. Shan, X. Song, M. Li, F. Yang, S. Xu, and A. Abubakar, "Physics embedded deep neural network for solving volume integral equation: 2-d case," *IEEE Transactions on Antennas and Propagation*, vol. 70, no. 8, pp. 6135–6147, 2021.

[17] Z. Ma, K. Xu, R. Song, C.-F. Wang, and X. Chen, "Learning-based fast electromagnetic scattering solver through generative adversarial network," *IEEE Transactions on Antennas and Propagation*, vol. 69, no. 4, pp. 2194–2208, 2020.

[18] T. Yin, C.-F. Wang, K. Xu, Y. Zhou, Y. Zhong, and X. Chen, "Electric flux density learning method for solving 3-d electromagnetic scattering problems," *IEEE Transactions on Antennas and Propagation*, vol. 70, no. 7, pp. 5144–5155, 2022.

[19] S. Qi, Y. Wang, Y. Li, X. Wu, Q. Ren, and Y. Ren, "Two-dimensional electromagnetic solver based on deep learning technique," *IEEE Journal on Multiscale and Multiphysics Computational Techniques*, vol. 5, pp. 83–88, 2020.

[20] T. Shan, J. Zeng, X. Song, R. Guo, M. Li, F. Yang, and S. Xu, "Physics-informed supervised residual learning for electromagnetic modeling," *IEEE Transactions on Antennas and Propagation*, vol. 71, no. 4, pp. 3393–3407, 2023.

[21] J.-Y. Wang and X.-M. Pan, "Physics-informed deep learning to solve 2d electromagnetic scattering problems," *The Applied Computational Electromagnetics Society Journal*, pp. 667–673, 2024.

[22] Z. Peng, B. Yang, Y. Xu, F. Wang, L. Liu, and Y. Zhang, "Rapid surrogate modeling of electromagnetic data in frequency domain using neural operator," *IEEE Transactions on Geoscience and Remote Sensing*, vol. 60, pp. 1–12, 2022.

[23] G. Cybenko, "Approximation by superpositions of a sigmoidal function," *Mathematics of control, signals and systems*, vol. 2, no. 4, pp. 303–314, 1989.

[24] J. Park and I. W. Sandberg, "Universal approximation using radial-basis-function networks," *Neural computation*, vol. 3, no. 2, pp. 246–257, 1991.

[25] B. C. Csáji *et al.*, "Approximation with artificial neural networks," *Faculty of Sciences, Etvs Lornd University, Hungary*, vol. 24, no. 48, p. 7, 2001.

[26] T. Chen and H. Chen, "Universal approximation to nonlinear operators by neural networks with arbitrary activation functions and its application to dynamical systems," *IEEE transactions on neural networks*, vol. 6, no. 4, pp. 911–917, 1995.

[27] S. R. Dubey, S. K. Singh, and B. B. Chaudhuri, "Activation functions in deep learning: A comprehensive survey and benchmark," *Neurocomputing*, vol. 503, pp. 92–108, 2022.

[28] K. Hornik, M. Stinchcombe, and H. White, "Universal approximation of an unknown mapping and its derivatives using multilayer feedforward networks," *Neural networks*, vol. 3, no. 5, pp. 551–560, 1990.

[29] Stinchcombe, "Universal approximation using feedforward networks with non-sigmoid hidden layer activation functions," in *International 1989 Joint Conference on Neural Networks*. IEEE, 1989, pp. 613–617.

[30] A. Pinkus, "Approximation theory of the mlp model in neural networks," *Acta numerica*, vol. 8, pp. 143–195, 1999.

[31] P. Kidger and T. Lyons, "Universal approximation with deep narrow networks," in *Conference on learning theory*. PMLR, 2020, pp. 2306–2327.

[32] T. Kim and T. Adali, "Universal approximation of fully complex feed-forward neural networks," in *2002 IEEE international conference on acoustics, speech, and signal processing*, vol. 1. IEEE, 2002, pp. I–973.

[33] F. Voigtlaender, "The universal approximation theorem for complex-valued neural networks," *Applied and Computational Harmonic Analysis*, vol. 64, pp. 33–61, 2023.

[34] X.-M. Pan, B.-Y. Song, D. Wu, G. Wei, and X.-Q. Sheng, "On phase information for deep neural networks to solve full-wave nonlinear inverse scattering problems," *IEEE Antennas and Wireless Propagation Letters*, vol. 20, no. 10, pp. 1903–1907, 2021.

[35] Z. Zhang, H. Wang, F. Xu, and Y.-Q. Jin, "Complex-valued convolutional neural network and its application in polarimetric sar image classification," *IEEE Transactions on Geoscience and Remote Sensing*, vol. 55, no. 12, pp. 7177–7188, 2017.

[36] C. Trabelsi, O. Bilaniuk, Y. Zhang, D. Serdyuk, S. Subramanian, J. F. Santos, S. Mehri, N. Rostamzadeh, Y. Bengio, and C. J. Pal, "Deep complex networks," *arXiv preprint arXiv:1705.09792*, 2017.

[37] M. Raissi, P. Perdikaris, and G. E. Karniadakis, "Physics-informed neural networks: A deep learning framework for solving forward and inverse problems involving nonlinear partial differential equations," *Journal of Computational physics*, vol. 378, pp. 686–707, 2019.

[38] L. Lu, X. Meng, Z. Mao, and G. E. Karniadakis, "Deepxde: A deep learning library for solving differential equations," *SIAM review*, vol. 63, no. 1, pp. 208–228, 2021.

[39] G. E. Karniadakis, I. G. Kevrekidis, L. Lu, P. Perdikaris, S. Wang, and L. Yang, "Physics-informed machine learning," *Nature Reviews Physics*, vol. 3, no. 6, pp. 422–440, 2021.

[40] M. Baldan, P. Di Barba, and D. A. Lowther, "Physics-informed neural networks for inverse electromagnetic problems," *IEEE Transactions on Magnetics*, vol. 59, no. 5, pp. 1–5, 2023.

[41] Y.-D. Hu, X.-H. W. H. Zhou, L. Wang, and B.-Z. Wang, "A more general electromagnetic inverse scattering method based on physics-informed neural network," *IEEE Transactions on Geoscience and Remote Sensing*, 2023.

[42] Y.-D. Hu, X.-H. Wang, H. Zhou, and L. Wang, "A priori knowledge-based physics-informed neural networks for electromagnetic inverse scattering," *IEEE Transactions on Geoscience and Remote Sensing*, 2024.

[43] W. Chew, M.-S. Tong, and H. Bin, *Integral equation methods for electromagnetic and elastic waves*. Springer Nature, 2022.

[44] W. C. Gibson, *The method of moments in electromagnetics*. CRC press, 2021.

[45] Y.-N. Liu and X.-M. Pan, "Solution of volume–surface integral equation accelerated by mlfma and skeletonization," *IEEE Transactions on Antennas and Propagation*, vol. 70, no. 7, pp. 6078–6083, 2022.

[46] S. Liang and R. Srikant, "Why deep neural networks for function approximation?" *arXiv preprint arXiv:1610.04161*, 2016.

[47] N. Ketkar, J. Moolayil, N. Ketkar, and J. Moolayil, "Introduction to pytorch," *Deep Learning with Python: Learn Best Practices of Deep Learning Models with PyTorch*, pp. 27–91, 2021.

[48] D. P. Kingma and J. Ba, "Adam: A method for stochastic optimization," *arXiv preprint arXiv:1412.6980*, 2014.

[49] K. He, X. Zhang, S. Ren, and J. Sun, "Delving deep into rectifiers: Surpassing human-level performance on imagenet classification," in *Proceedings of the IEEE international conference on computer vision*, 2015, pp. 1026–1034.